



**HAL**  
open science

# Simulation of large dimensional reinforced and prestressed concrete structures using a new adaptive static condensation method including automatic mesh partitioning

Ali Mezher, Ludovic Jason, Gauthier Folzan, Luc Davenne

## ► To cite this version:

Ali Mezher, Ludovic Jason, Gauthier Folzan, Luc Davenne. Simulation of large dimensional reinforced and prestressed concrete structures using a new adaptive static condensation method including automatic mesh partitioning. *Finite Elements in Analysis and Design*, 2022, 202, pp.103718. 10.1016/j.finel.2021.103718 . hal-03510952

**HAL Id: hal-03510952**

**<https://hal.science/hal-03510952>**

Submitted on 4 Aug 2023

**HAL** is a multi-disciplinary open access archive for the deposit and dissemination of scientific research documents, whether they are published or not. The documents may come from teaching and research institutions in France or abroad, or from public or private research centers.

L'archive ouverte pluridisciplinaire **HAL**, est destinée au dépôt et à la diffusion de documents scientifiques de niveau recherche, publiés ou non, émanant des établissements d'enseignement et de recherche français ou étrangers, des laboratoires publics ou privés.

# Simulation of large dimensional reinforced and prestressed concrete structures using a new adaptive static condensation method including automatic mesh partitioning

*A. Mezher<sup>\*,&, †</sup>, L. Jason<sup>&</sup>, G. Folzan<sup>&</sup> and L. Davenne<sup>†</sup>*

<sup>&</sup> Université Paris-Saclay, CEA, Service d'Études Mécaniques et Thermiques, 91191, Gif-sur-Yvette, France

E-mail: [ali.mezher@cea.fr](mailto:ali.mezher@cea.fr), [ludovic.jason@cea.fr](mailto:ludovic.jason@cea.fr), [gauthier.folzan@cea.fr](mailto:gauthier.folzan@cea.fr), web page: <http://www.cea.fr>

<sup>†</sup> LEME, UPL, Université Paris Nanterre, 92410 Ville d'Avray, France

Email: [luc.davenne@parisnanterre.fr](mailto:luc.davenne@parisnanterre.fr) - Web page: <http://www.leme.parisnanterre.fr>

## ABSTRACT

In order to evaluate the cracking process in large reinforced and pre-stressed concrete structures, a predictive simulation of concrete damage with a refined mesh and a nonlinear law is required. Because of the computational load, such modelling is not applicable directly on large-scale structures whose characteristic dimensions are over several tens of meters. To deal with this type of structure, an adaptive static condensation method (ASC), which concentrates the computational effort on the damaged area (domain of interest) only, is proposed. The ASC method is first presented. A particular attention is paid to the needed developments to extend its domain of application up to prestressed concrete structures. The method is then applied to a three point bending prestressed beam and validated by comparison to a classical finite element damage computation. The numerical efficiency of the proposed approach is evaluated with, on this application, a time saving factor of about 15.

An automatic mesh partitioning method is then implemented to make the method even more efficient. Based on physical considerations, it takes into account the expected shape and the evolution of the damaged regions during the loading. It is applied to three test cases with different geometries and loading to discuss the calibration process through a sensitivity analysis. A unique set of parameters is finally proposed and the efficiency of the method is demonstrated. As a conclusion; a complete automatic method is made available for the simulation of large scale reinforced and prestressed concrete structures

**Keywords:** reinforced and prestressed concrete, large structures, static condensation, damage

## 1. INTRODUCTION

Numerical simulation is playing an increasingly role in engineering sciences in order to facilitate the design of new structures while limiting the production of experimental prototypes. The ever-increasing need to consider more and more complex phenomena in order to predict as accurately as possible the behavior of a structure in all situations very quickly leads to highly complex models. On large structures, these approaches are prohibitively expensive and thus typically inapplicable to modelling the overall structural response. In practice, engineers are interested by the fine physical description only in very specific areas rather than by the response throughout the whole structure. The need for a "reduced" method and/or to reduce the computational cost is very often necessary.

The physical phenomenon, which is studied in this contribution is the cracking in concrete structures which occurs on a relatively local scale. Its modeling thus requires a fine mesh and a nonlinear constitutive law to obtain representative results. However, applying this fine density of mesh (order of centimeter) directly to large-scale structures (e.g. containment buildings) is challenging, because of prohibitive computation times and memory occupancy [1].

The decomposition of the system combined to the use of parallel computation to exploit several computation units simultaneously is one of the possible solutions. It can significantly reduce the calculation time. Several approaches have been developed for parallel computation analysis. A review of the fundamental concepts and issues of parallel processing is made in [2]. The parallel processing can be applied in fluid mechanics [3], for nonlinear analysis of reinforced concrete three-dimensional frames [4] or on structural dynamics in [5], among others domains. Parallelism brings a computing power and a storage capacity, which increases with the increase of the number of processors. This makes it possible to reach higher simulation levels, within a reasonable timeframe [6]. However, with this type of approach, the overall computational load increases because of the cost of communication between the different calculation units. Therefore, for a given computing power, this method does not improve the computation. The adaptive mesh refinement, introduced initially in [7] is another possible solution. It consists in locally increasing the density of the mesh in the zones where it is essential to calculate the solution with greater precision. The advantage of the method lies mainly in its performance in terms of memory size and CPU time [8]. However, with this approach, the nonlinear behavior is verified on the whole structure, even in the non-interesting areas with linear behavior. In the case of localized damaged zones, this step can become very costly, and the solution is not totally satisfying. In computational mechanics, static condensation is a model reduction method that reduces the number of degrees of freedom by eliminating variables from the linear system in the stiffness matrix. Condensed substructures are thus created. "Super-elements" are generally defined by eliminating the internal unknowns in the condensed zones. Complex problems, whose complexity is related to their size, can be calculated at a more reasonable cost. The condensation method was first introduced by Guyan in 1965 [9] and has been widely used in mechanics. The method is called "static condensation" since it is only exact for static problems, even if it has been widely applied in structural dynamics. In this case, the condensation of mass is approximated [9]. The initial formulation have been gradually improved in dynamic calculations ([10], [11], [12]) and/or associated with substructuring ([13]) in the analysis of structures with localized nonlinearities. In [13], the static condensation was used for efficient conceptual-level aerospace structural design. Regarding nonlinear cracking in reinforced concrete structures, a so-called "adaptive static condensation" method has been developed [15] (ASC method). It consists in concentrating the computational effort of the nonlinear calculation on preliminary defined "zones of interest" (zones with expected cracking behavior), by "eliminating" the zones with a linear elastic behavior. This approach uses Guyan's static condensation method [9] to replace the elastic zones by a set of boundary conditions applied at the boundaries of the zones of interest. As the system evolves (evolution of a given crack or apparition of a new one), criteria are used to detect if damage is likely to appear and to make evolve the geometry of the zones of interest. This method enables to reduce the dimension of the nonlinear problem without altering the quality of the results compared to a complete reference computation. However, the domain of applicability of the method was initially limited to reinforced concrete structures and included a significant number of "user parameters".

The aim of this contribution is first to improve this method in terms of domain of applicability. Concrete is indeed a material which is well-resistant to compression but rather limited in case of tension loads. That is why in several applications, concrete may be prestressed by means of steel cables, that maintains the concrete stress in compression even in case of tensile loads [16]. Numerical simulation of this process may be a difficult task, if a representative state of stress wants to be achieved. It is indeed necessary to deal with the first steps of application of the tension, the immediate loss of the prestressing, the behaviour under external loads and, in the case of long term analysis, the loss of prestressing due to phenomena such as shrinkage and creep of concrete, and relaxation of tendons [14].

After a brief description of the ASC method, it is thus proposed to enlarge its field of application to prestressed concrete structures in section 2. To increase the numerical efficiency and to limit the number of additional parameters, an automatic mesh partitioning method is then developed in section 3. It is applied on three test cases through a sensitivity analysis to argue the proposition of a unique set of parameters, which consolidates the proposition of a fully automatic and numerically efficient adaptive static condensation method.

## 64 2. ADAPTIVE STATIC CONDENSATION (ASC)

### 65 2.1 METHOD AND IMPLEMENTATION

66 The principle of the initial static condensation method is first briefly summarized. The modifications to obtain an  
67 “adaptive” static condensation are then discussed. Finally, the developments to be applied to prestressed concrete  
68 structures are presented and validated on a representative test case.

#### 69 2.1.1 Principle of static condensation

70 For a given mechanical problem, the static equilibrium can be expressed in matrix form by the equation:

$$K u = f \quad (1)$$

71 with  $K$  the stiffness of the structure,  $f$  the force vector and  $u$  the displacement vector. Guyan's approach [9] consists  
72 in breaking down the structure into two domains: a master domain  $\Omega_M$ , which will remain totally represented and a  
73 slave one  $\Omega_C$ , which will be condensed.

74 Differentiating the degrees of freedom (DOF) into the slave and the master domains, equation (1) becomes:

$$\begin{pmatrix} K_{C,C} & K_{C,M} \\ K_{M,C} & K_{M,M} \end{pmatrix} \begin{pmatrix} U_C \\ U_M \end{pmatrix} = \begin{pmatrix} f_C \\ f_M \end{pmatrix} \quad (2)$$

75 Let  $n$  be the number of DOF of the total system and let  $p$  and  $q$  respectively be the number of slave and master  
76 DOF with  $n = p + q$ ,  $K_{C,C} (\in \mathbb{R}^{p,p})$ ,  $K_{M,M} (\in \mathbb{R}^{q,q})$ ,  $K_{M,C} (\in \mathbb{R}^{p,q})$  and  $K_{C,M} (\in \mathbb{R}^{q,p})$  are the stiffness matrix related to  
77 respectively the slave domain, the master domain, the master-slave connections and the slave-master connections.  
78  $U_C (\in \mathbb{R}^p)$  and  $U_M (\in \mathbb{R}^q)$  are respectively the slave and master DOF.  $f_C (\in \mathbb{R}^p)$  and  $f_M (\in \mathbb{R}^q)$  are the external forces  
79 applied to  $\Omega_C$  and  $\Omega_M$  respectively.

80  
81 By developing equation (2), a reduced (condensed) problem can be defined by:

$$\tilde{K} \cdot U_M = \hat{F} \quad (3)$$

82 The reduced stiffness matrix  $\tilde{K}$  and the condensed force are given by:

$$\begin{cases} \tilde{K} = K_{M,M} - K_{M,C} K_{C,C}^{-1} K_{C,M} \\ \hat{F} = f_M - K_{M,C} K_{C,C}^{-1} f_C \end{cases} \quad (4)$$

83 As expected, the dimension of the reduced system is equal to  $q$  which is less than  $n$  and its resolution gives the  
84 solution on the master domain  $\Omega_M$ . It should be noted here that the matrix  $\tilde{K}$  can be denser than classical resolution  
85 matrices, in particular at the master points. It can thus add difficulties to solve this reduced system. Then, storing a  
86 dense matrix can also be more expensive in terms of memory than a sparse one. However, even considering these  
87 potential drawbacks, in main cases, the resolution of the reduced system remains faster than that of the global  
88 system, in particular when the condensed part is large compared to the non-condensed one.

89 However, it remains possible to determine the vector  $U_C$  by applying a “decondensation”:

$$U_C = K_{C,C}^{-1} (f_C - K_{C,M} \cdot U_M) \quad (5)$$

90 It is noted that if the domain  $\Omega_C$  is large, the dimension of the inverse term  $K_{C,C}^{-1}$  is large and its computation can  
91 become expensive.

#### 92 2.1.2 The ASC method: principle and algorithm

93 The adaptive static condensation method [15] is a method for the resolution of large-dimensional structures with  
94 non-linear behavior and with localized damage zones, which can evolve. Based on the main principle of the initial  
95 static condensation method, the global idea consists in cutting the problem into zones, fully representing the zones  
96 with expected nonlinear behavior, condensing the zones with linear elastic behavior and reassuring during the  
97 calculation that the condensed zones remain elastic. If the last step is not fulfilled, new zones of interest have to be  
98 included and fully represented in the calculation and some steps will be calculated to keep the accuracy of the  
99 computation. That is why the method have been called “adaptive” condensation method. It is to be noted that the  
100 ASC method is expected to be particularly efficient when the cracking behavior is localized over an area of small  
101 dimensions compared to the size of the entire structure. The more localized the damage, the more efficient the  
102 method. On the contrary, the interest of the ASC method may be limited when damage appears from the beginning  
103 of the calculation on large zones, as it may lead to the activation of the whole structure. Figure 1 represents the  
104 algorithm of the ASC method. This algorithm has two phases: a setup phase and a calculation phase.

##### 105 2.1.2.1 Setup phase

106 The first step is to cut the structure into zones (Figure 2-a). It is to be noted that in the original method [15], this  
107 initial geometric decomposition is fully given by the user. This point will be discussed in section 3. Each zone is  
108 then condensed and replaced by equivalent boundary conditions on its borders (“first condensation”). This  
109 condensation of stiffness and loading is done only once during the setup phase and the condensed matrices are  
110 saved and used when needed during all the simulation. At the same time, a linear elastic computation is performed  
111 on the entire structure to identify an initial domain of interest (DI), which corresponds to the domain that will be

112 activated and totally represented. This DI is obtained from a predefined criterion based on the Mazars's equivalent  
 113 deformation [16]. More details about this choice will be detailed in 3.2. The rest of the structure is called the elastic  
 114 domain (ED).  
 115 The "second condensation" builds equivalent boundary conditions on the borders between the DI and the ED  
 116 (Figure 2-d). The nonlinear computation is finally performed on the DI only, associated to the equivalent stiffness  
 117 boundary conditions. This system has a size smaller than the complete structure, which improves the performance  
 118 of computation [15].

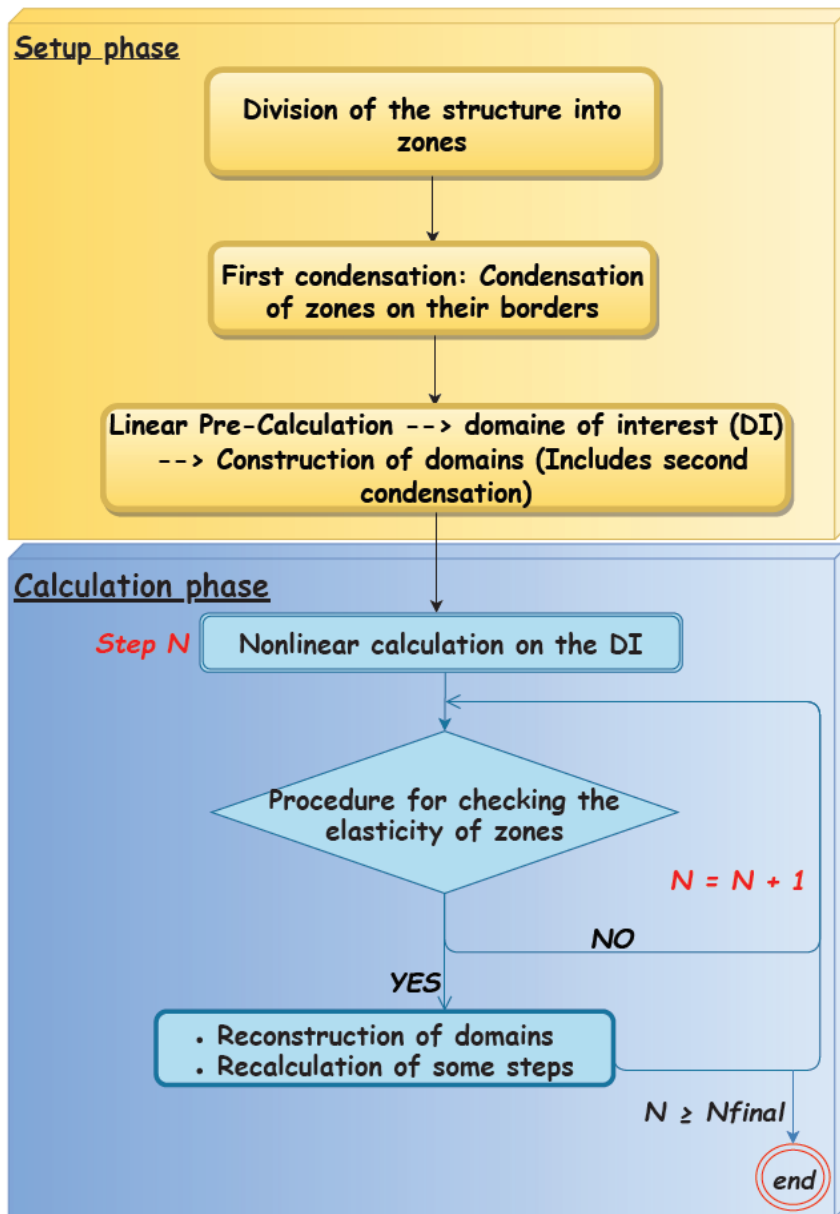


Figure 1 : simplified algorithm of the ASC method

119  
120

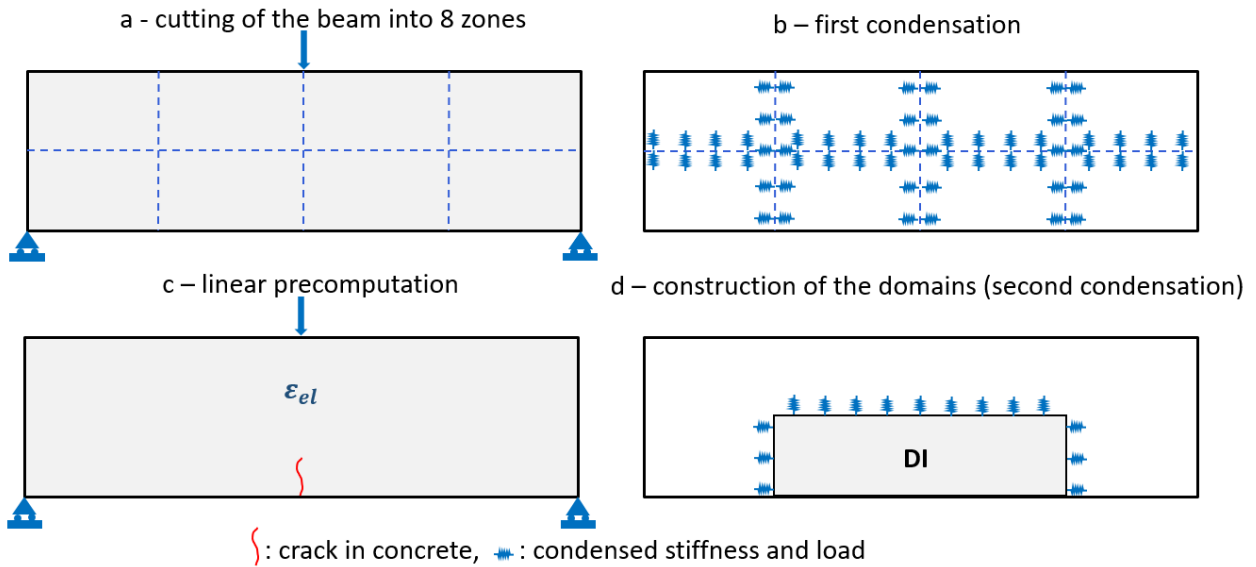


Figure 2 : Setup phase on a single beam in bending

121  
122

123 2.1.2.2 Calculation phase

124 The non-linear computation remains representative as long as the condensed zones remains elastic. This  
125 hypothesis is checked periodically and the zones of interest may evolve if necessary during the computation. This  
126 procedure includes two verification criteria (see Figure 3). In this figure,  $N$  is the current step number,  $i$  is a natural  
127 integer and  $p$  is a parameter which determines the number of steps after which the initiation criterion is verified.

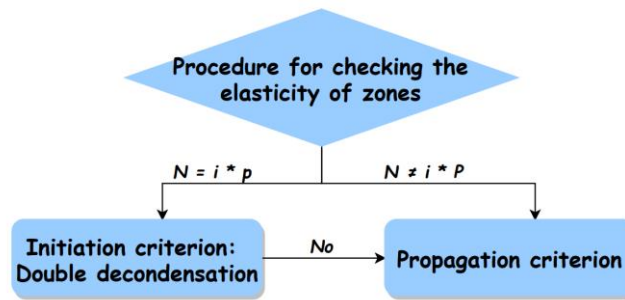


Figure 3 : procedure of checking the elasticity of zones

128  
129

- 130 • **The propagation criterion** (Figure 4) evaluates the potential propagation of existing zones of interest to  
131 neighboring condensed zones. It detects if the damage is approaching the border of the DI. Propagation  
132 bands are defined over a width  $L$  around the border of the DI (Figure 4 – a). If damage reaches this band,  
133 the neighboring zone is added to the DI (Figure 4 - b). As this test is only geometric, the associated  
134 computational cost is not expensive. This criterion is thus checked at the end of each time step.

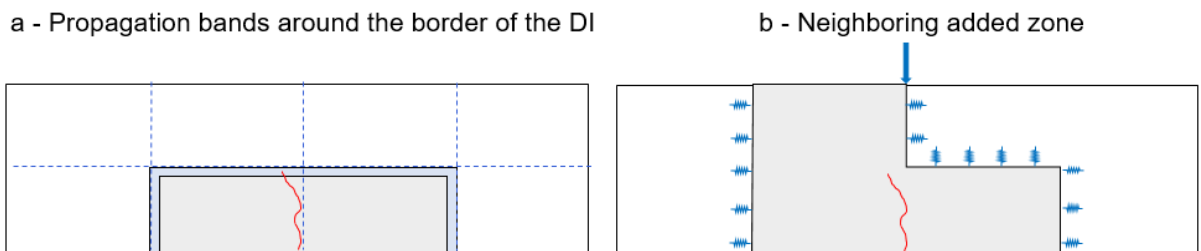


Figure 4 : Propagation criterion and evolution of the DI

135  
136

- 137 • **The initiation criterion** (Figure 5) evaluates the potential apparition of new zones of interest  
138 (corresponding to the apparition of new damaged zones). It supposes to check the elasticity of the  
139 condensed zones. To do so, a double “decondensation” is performed to obtain the values of the  
140 displacements on the whole structure (not only in the DI). Elasticity hypothesis is verified from the  
141 calculation of the inelastic deformation  $\varepsilon_{inel} = \varepsilon - \varepsilon_{el}$  with  $\varepsilon$  is the strain calculated using the used  
142 constitutive law and the stress state and  $\varepsilon_{el}$  is the elastic strain calculated using the displacement field  
143 obtained. If  $\varepsilon_{inel} > 0$  in a given zone, outside the DI, this zone has to be included in the new DI. Because  
144 of the cost of the double “decondensation”, this criterion is only checked each  $p$  loading step, where  $p$  is  
145 an integer chosen by the user in the initial method.

146

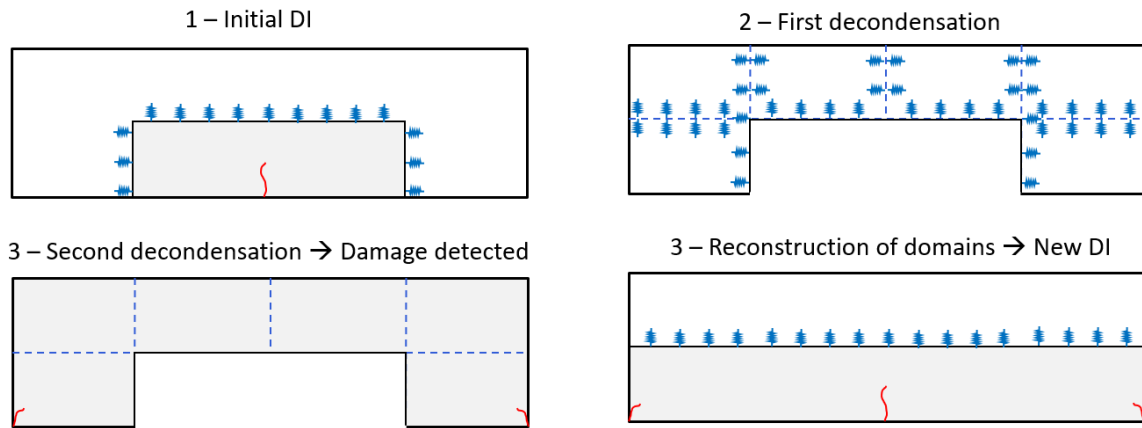


Figure 5 : Initiation criterion and evolution of the DI

147  
148

149 In both cases (propagation and initiation), if the DI evolves, a domain reconstruction procedure is used in which  
150 only the second condensation is carried out. It especially shows the advantage of the double condensation as a re-  
151 condensation of the whole structure is not needed. It is to be noted that in both cases, if the DI is changed, previous  
152 loading steps need to be recalculated ( $p$  steps in case of initiation, one step for propagation). Details can be found  
153 in [15].

## 154 2.2 EXTENSION FOR PRESTRESSED CONCRETE STRUCTURES

### 155 2.2.1 Modification to the ASC method

156 In its original form, the ASC method was limited to reinforced concrete structures. In this section, its application to  
157 prestressed concrete structures is discussed.

158 Concrete resists well in compression, but has a little tensile strength. It must therefore be artificially compressed in  
159 the tensioned areas, so that the concrete remains compressed or very slightly tensioned, to avoid cracking. The  
160 term “prestressed” indicates that the concrete is put into compression in its “initial state”. In the following, the  
161 application of the ASC method to the calculation of post-tensioned prestressed structure is developed.

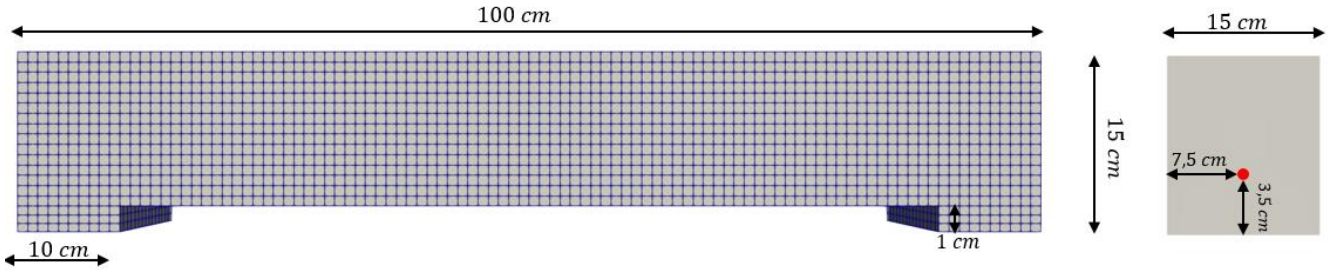
162  
163 The first step in the numerical prestressing process consists in evaluating the tension profile along the tendons.  
164 Tension losses are considered which may result from linear and angular friction, anchor retreat or steel relaxation  
165 and they are calculated, according to Eurocode 2 standards [17].

166 The tension profile (stress) is first changed into a field of nodal forces on the cable. These nodal forces are then  
167 applied to the structure without considering the stiffness of the cables. A mechanical equilibrium is reached through  
168 an iterative nonlinear process. A second mechanical equilibrium is then obtained, taking into account the stiffness  
169 of the cables, the values of the prescribed stresses in the cables and the stress distribution in the concrete, which  
170 has been obtained from the first equilibrium. Details can be found in [18]. It is to be noted that compared to simpler  
171 alternative methods for prestressing applications (initial temperature field, external compressive load...), this  
172 approach enables to obtain the appropriate values of the stress inside concrete (in compression) and cables (in  
173 tension). Moreover, this method makes it possible to apply the tension in several steps of computation (which is  
174 beneficial in the case of non-linearity) or to stretch the cables successively (one after the other).

175 As the nonlinear computations on the whole structure may be time consuming, the presented numerical  
176 prestressing process is adapted to the ASC method. The zones of the structure which contain the ends of cables  
177 builds the initial DI (maximum of the stress in concrete). The prestressing stress in the condensed zones are then  
178 replaced by a prestressing load which is condensed at the border of the DI. A verification is finally done at the end  
179 of the computation to check the elasticity of the initially condensed domain (ED) and additional steps of calculations  
180 are carried out in case of appearance of damage in new zones following the application of prestressing.

### 181 2.2.2 Example of application

182 A 1 m long beam is considered. A condensed calculation is performed and compared to a classical finite element  
183 simulation. Both computations are done using the finite element code Cast3m [18] on the same computing node  
184 (24 cores). This beam, whose dimensions are given in Figure 6 is modeled in three dimensions (3D). The concrete  
185 mesh is made up of 23400 linear cubic elements (1 cm side) and the steel tendon is modeled using 100 bar  
186 elements (1cm length). These bar elements have an equivalent section of  $S = 7.0 \text{ cm}^2$  (diameter 3 cm). Concrete  
187 is modeled using Mazars’s damage model [19] with the same parameters as in [20]. The parameters used give a  
188 compressive strength of 41.4 MPa at 28 days and a tensile strength of 3.03 MPa. A nonlocal integral method [21]  
189 is used to limit the damage mesh dependency in concrete with an internal length  $L_c = 3 \text{ cm}$ . A linear elastic model  
190 is considered for the tendon, as a plastic behavior is not expected during the loading. The cable is tensioned by its  
191 two ends with a force  $P = 20 \text{ kN}$ . The bond between the tendon and the concrete is ensured by kinematic  
192 conditions between the degrees of freedom of the nodes of the cable and those of the associated concrete elements  
193 (perfect adhesion).



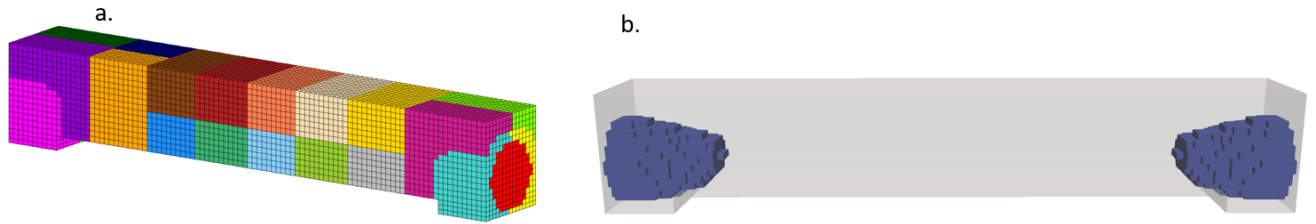
• **Prestressed cable of diameter 3 cm**

**Cross section**

194  
195

Figure 6 : prestressed concrete beam: mesh of the concrete (left), and cross section (right))

196 The structure is partitioned into 22 zones using the automatic mesh partitioning procedure that will be presented in  
197 the next part of the paper. This particular mesh decomposition does not affect the validation process but only  
198 impacts the numerical performance. Figure 7-a shows the resulting partitioned structure. As previously mentioned,  
199 the initial DI is defined as the concrete zones including the ends of the tendon (Figure 7 -b).

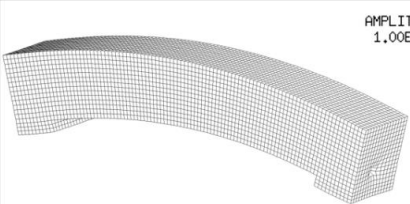
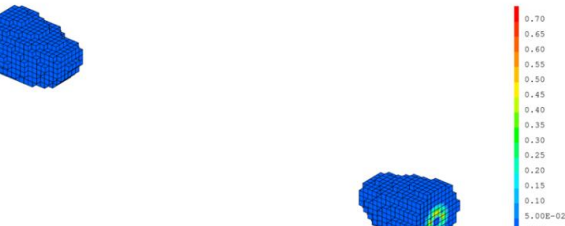


200  
201

Figure 7 : a- decomposition of the beam on initial zones, b- initial domain of interest in blue (DI)

202 Figure 8 shows the results of the two calculations. Damage appears in both cases around the ends of the tendon.  
203 It was expected as this damage results from the singularity of stresses due to the application of the tension on a  
204 single node of the 1D cable ([22],[23] and [24]). This numerical aspect is a well-known limit of the proposed  
205 numerical prestressing process. It could be avoided using for example a cone of stress diffusion to distribute the  
206 tension force over a larger concrete surface [25]. However, this consideration is out of the scope of this paper.  
207 The same results are obtained between both calculations. Figure 9 shows that in DI, the same forces were obtained  
208 along the cable in the condensed calculation as the complete reference calculation. This validates the application  
209 of the ASC method for the calculation of prestressed structures. The numerical efficiency results of the ASC method  
210 are given in Table 1. A time saving factor of 15.9 is observed in this case. This numerical efficiency is directly related  
211 to the number of “nonlinear” degrees of freedom (3680 DOF with the ASC method against 27381 in the complete  
212 calculation). It is noted that this case may represent the most beneficial case for the ASC method as the damage  
213 is much localized and does not evolve. The ASC method thus concentrates the non-local nonlinear effort only on  
214 limited geometric zones, compared to the classical calculation which supposes to check the nonlocal criterion on  
215 the whole structure.  
216

217

	Calculation on the complete structure	Calculation with the ASC method on the DI
Deformations		
Damage profiles		

217  
218

Figure 8 : results of calculations on the prestressing beam

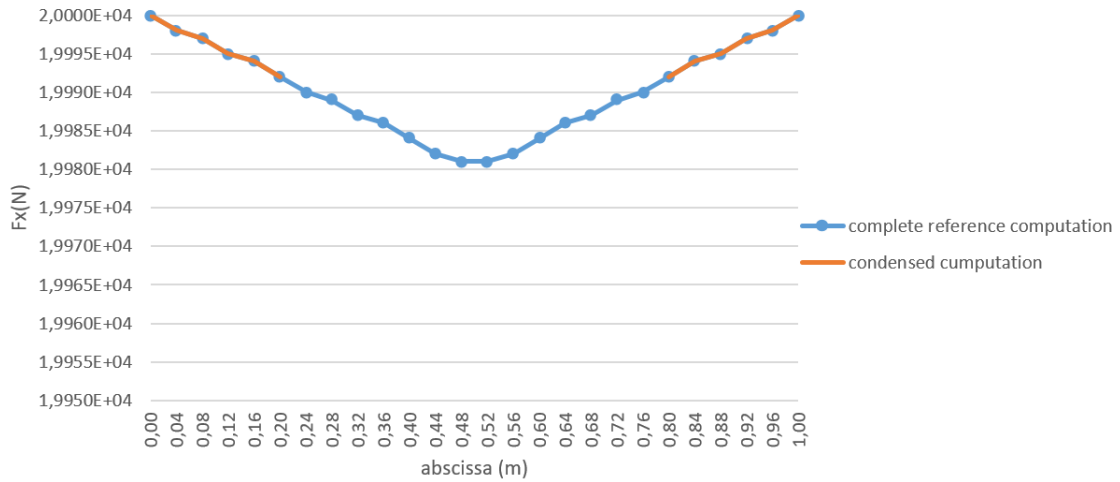


Figure 9: longitudinal force along the cable at the end of prestressing

Table 1 : Numerical efficiency results on the prestressing beam

	Complete calculation	Calculation with the ASC
Processor time	1685 s	105 s
Gain factor	-	15,94
Number of degrees of freedom	27381	3680

### 3. AUTOMATIC MESH PARTITIONING METHOD

#### 3.1 EFFECT OF MESH PARTITIONING ON THE COMPUTATION TIME

The ASC method supposes an initial decomposition of the mesh into zones. In its original form, this decomposition is arbitrarily provided by the user. However, this step can deeply affect the computational performance of the method. To illustrate this impact, a notched bending beam is considered with several initial mesh partition using the ASC method. The beam is 160 cm long and 40 cm high including a notch at mid span, which is 80 mm high and 8 mm large. It is modeled in two dimensions (plane stress with thickness of 20 cm). The mesh is made with 6440 quadrilateral elements of 1 cm length (Figure 10). Mazars's model is chosen, considering the same parameters and the same regularization technique as in section 2.2. The load is applied on a 10 cm zone on the top of the beam, through an imposed vertical displacement downwards increasing from 0 up to 25 mm. Vertical displacement is blocked at the support points and horizontal displacement is blocked at the top middle point only and free elsewhere.

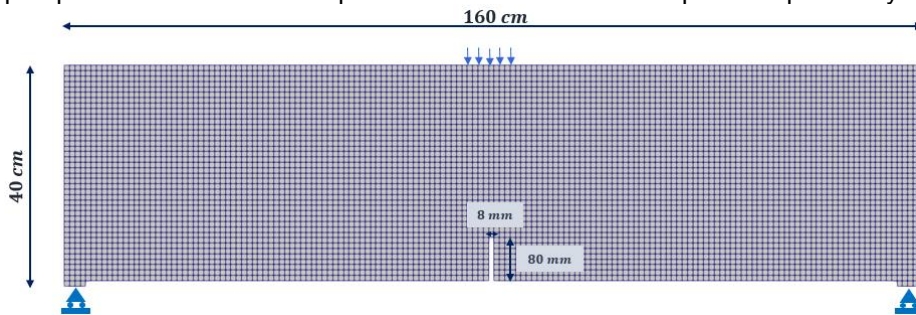


Figure 10 : details of the beam (mesh and dimensions)

Figure 11 illustrates the different initial partitions (zones of equivalent sizes) which are considered for each computation using the ASC method. 10 calculations are performed. Each calculation corresponds to a division of the total structure into  $N$  equivalent zones with  $N \in \{1, 2, 4, 8, 16, 32, 64, 128, 256, 512\}$ . The calculations are performed on the same computer to compare the calculation time.

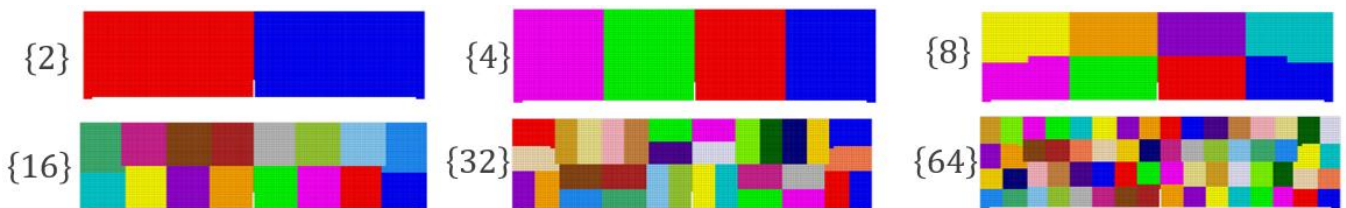
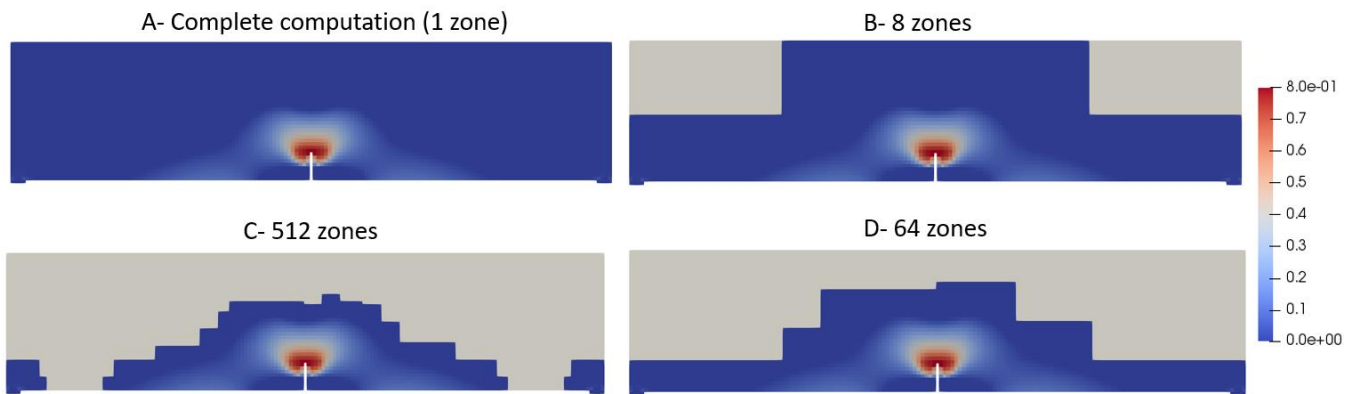
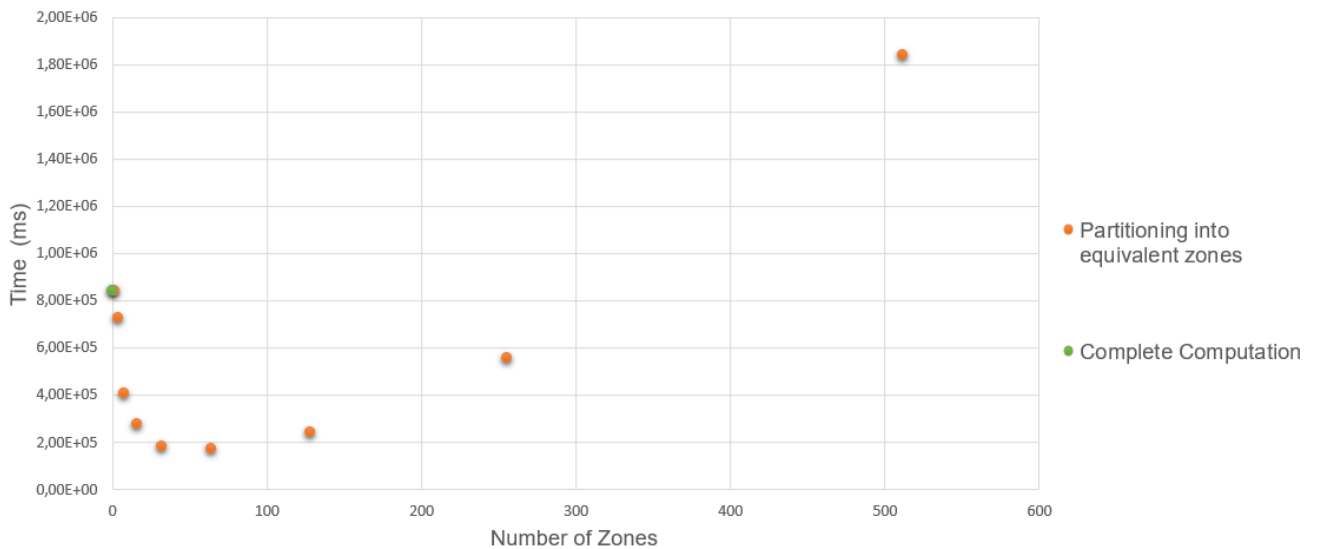


Figure 11 : Examples of initial mesh decomposition into 2, 4, 8, 16, 32 or 64 equivalent zones

242 The results of the 10 calculations are first compared in terms of damage distribution. Identical results are obtained.  
 243 Figure 12 illustrates the damage profile at the end of the computation for N = 1 (non-condensed complete  
 244 computation), 8, 512 and 64 zones. Table 2 details the computation results for these four decompositions. The  
 245 complete calculation has 321 computation steps. In the 8 zones case, a large part of the domain of interest is, in  
 246 fact, not damaged. This case has 327 steps. For the case of 512 zones, almost the whole DI is damaged (optimized  
 247 DI) but 412 steps of computation were necessary. As a conclusion, dividing into very small zones optimizes  
 248 the size of the domain of interest (DI) during the computation but requires more steps (propagation of damage,  
 249 reconstruction of domains and recalculations of some steps). A division into large zones reduces the number of  
 250 computation steps but increases the size of the DI. We also notice that the best partitioning (64 zones) is that which  
 251 makes a compromise between the size of the activated domain and the number of steps of computation.  
 252 Figure 13 gives the calculation time obtained as a function of the number of initial partitioning zones. This graph  
 253 shows that the mesh partitioning significantly affects the computation time with the ASC method. For example,  
 254 for the case of 512 zones, the computation is approximately 2 times slower than the complete computation while for  
 255 the optimal case (64 zones), the computation is approximately 5 times faster. These differences can be explained  
 256 by the concurrence between the size of the domain of interest (which may be smaller with a decomposition into a  
 257 larger number of zones) and the propagation and initiation criteria (which may be activated more often in the  
 258 condensed computation if the size of the initial zones are small).



259  
 260 *Figure 12 : damage profiles at the end of the computation for different initial mesh decomposition (grey zones are remaining*  
 261 *condensed ones)*



262  
 263 *Figure 13: calculation time as a function of the number of partitioning zones*

264 *Table 2 : calculation details for different mesh decomposition (1, 8, 512 and 64 zones)*

Number of zones	1 (complete computation)	8	512	64
Size of the DI % total size	100%	74%	32%	44%
Number of steps	321	327	412	342
Time (s)	$8,39 \times 10^2$	$4,07 \times 10^2$	$18,4 \times 10^2$	$1,73 \times 10^2$

265

266 This study clearly indicates that the initial partition method has a significant influence on the computational  
 267 efficiency. In addition, we have no prior knowledge on the number of zones that gives the optimal computation time.  
 268 That is why a new mesh-partitioning method has been developed. In the state-of-the-art, the existing methods of  
 269 mesh partitioning are not fully suitable as they aim rather at distributing the numerical difficulty (therefore the non-  
 270 linearity) between the zones to achieve a balanced estimate of execution time across the processors in a distributed  
 271 system [26] [27] [28]. If this strategy is suitable for methods like parallel computation for example, they are not fully  
 272 adapted to the proposed ASC method, as the goal is here to concentrate the computational effort in the domains  
 273 of interest only. It becomes thus necessary to develop a suitable automatic partitioning method.

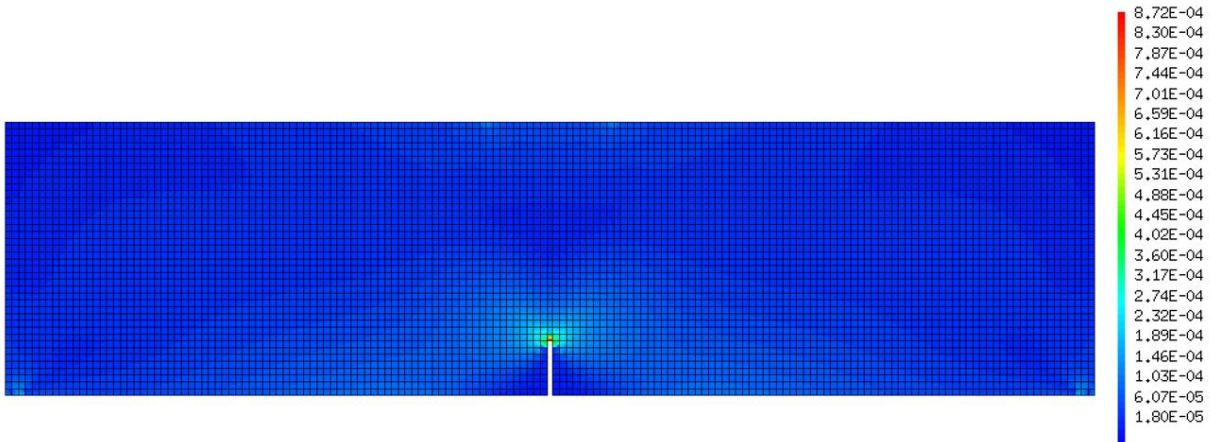
### 274 3.2 METHOD

275 The automatic mesh partitioning method is presented in this section, based on physical considerations of damage  
 276 initiation and propagation. It is developed so as to be applicable to different types of structures and loads. For the  
 277 aim of simplicity, it is illustrated on the notched bending beam used in the previous section. The method is  
 278 decomposed into five steps:

- 279 1. The first step consists in carrying out a linear precomputation on the whole structure to obtain a distribution  
 280 of the elastic strain. The maximum of the loading is used as the applied force for the linear precomputation.  
 281 In the case where only one type of loading is considered, this level does not affect the results because the  
 282 steps of the partitioning method are carried out using relative quantities. In the case of several types of  
 283 loadings (prestressing followed by an internal pressure for example), the force used for the precomputation  
 284 is the combination of the maximum values of each loading in order to take into account the potential  
 285 interactive effects. This choice may not be the optimal one for every configuration. However, it is to be  
 286 noted that the impact would be on the mesh partition and not on the result of the mechanical simulation. A  
 287 quantity of interest is then calculated to partition the structure. In this contribution, related to damage  
 288 mechanics, this quantity is Mazars's equivalent strain,  $\varepsilon_{eq}$ , which is computed using the following equation:

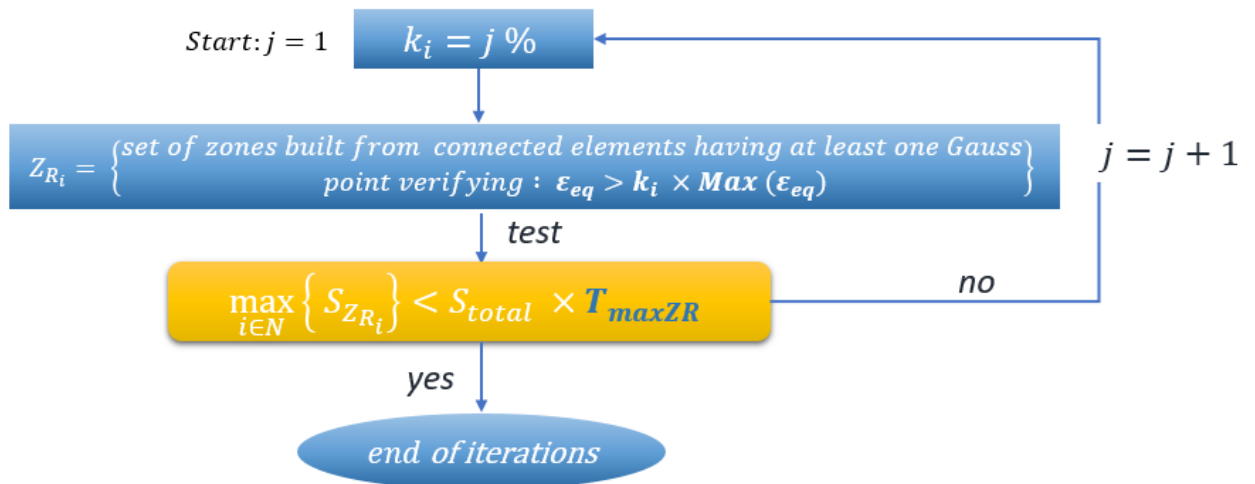
$$\varepsilon_{eq} = \sqrt{\langle \varepsilon_1 \rangle_+^2 + \langle \varepsilon_2 \rangle_+^2 + \langle \varepsilon_3 \rangle_+^2} \quad (6)$$

289 Where  $\langle \varepsilon_i \rangle_+$  represents the principal positive value of the strain. As an illustration, Figure 14 shows the  
 290 elastic equivalent strain  $\varepsilon_{eq}$  obtained on the beam for an imposed displacement downward equal to 25 mm.  
 291 It is to be noted that different quantities of interest could have been considered like Von Mises or Tresca  
 292 stresses, according to the constitutive law used.



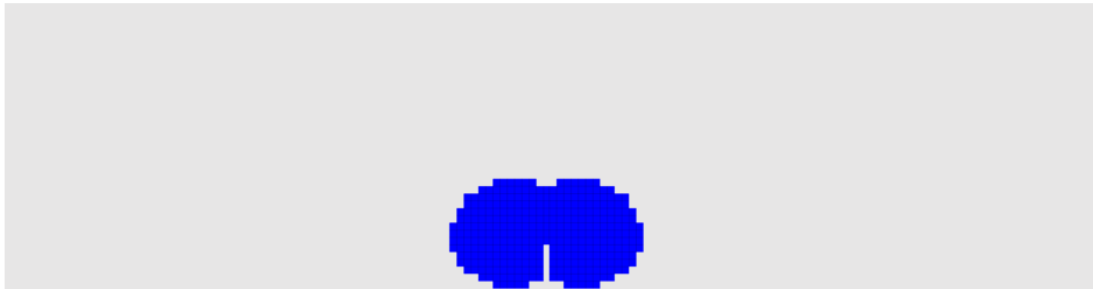
293 *Figure 14: distribution of elastic  $\varepsilon_{eq}$  on the notched bending for an imposed displacement of 25 mm.*

- 295 2. The second step is related to the definition of the zones which are most likely to be damaged ("risky zones").  
 296 They are obtained using an iterative approach, which is illustrated in Figure 15. In this figure,  $S_{total}$  is the  
 297 total surface of the structure and  $S_{ZR}$  is the total surface of the expected risky zones.  $T_{maxZR}$  is the first  
 298 parameter of the method, that defines the maximum goal size of a risky zone compared to the total size of  
 299 the structure. To do so, the iteration process is initiated considering all the connected elements in which at  
 300 least one Gauss point has an equivalent strain ( $\varepsilon_{eq}$ ) greater than 1% of the maximum equivalent strain  
 301 ( $\max(\varepsilon_{eq})$ ). This obviously gives very large areas (roughly the whole structure). As the "stop" criterion is  
 302 not met, this percentage is gradually increased, until the convergence is obtained. The obtained initial risky  
 303 zone on the notched beam is illustrated in Figure 16.



304  
305

Figure 15 : iterative approach for the identification of risky zones



306  
307  
308

Figure 16 : Application of the iterative method for the determination of the risky zone on the notched bending beam (for a value of  $T_{maxZR} = 3 \%$ )

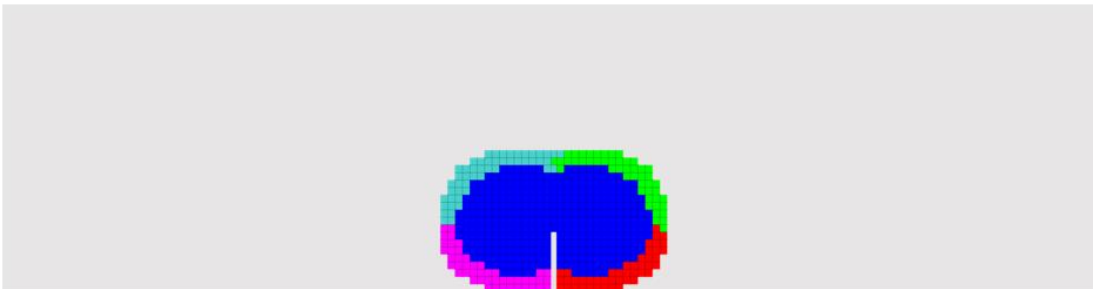
309  
310  
311

- The areas surrounding each “risky zone” are then considered as potential propagation zones. It introduces the second parameter of the method,  $T_{Zpr}$ , such as the size of the potential propagation zone  $S_{Zpr_i}$  (corresponding to the risky zone  $ZR_i$ ) reaches:

$$S_{Zpr_i} = \frac{S_{ZR_i}}{T_{Zpr}} \quad (7)$$

312  
313  
314  
315  
316  
317

The shape of these zones is first obtained supposing a uniform radial propagation of the damage. In order to take into account a potential directional propagation of the damage, each propagation zone is then cut into  $N_{partpr}$  zones (with  $N_{partpr}$  the third parameter of the method). This choice enables to activate in the ASC method, only a part of the surrounding area in case of a directional propagation, while not penalizing computational time in case of radial progression as all the surrounding zones will be activated at the same time. This step is illustrated for the notched bending beam in Figure 17.



318  
319

Figure 17 : the propagation zones obtained on the notched beam for a value of  $T_{Zpr} = 4$  and  $N_{Partpr} = 4$

320  
321  
322

- The rest of the structure is finally divided into equivalent zones by minimizing the number of points on the borders using the “nested dissection” algorithm [29] . This algorithm allows the structure to be divided into  $2^n$  zones of equivalent size. The approximate size of each remaining zone  $S_{Zrest}$  is chosen such as

$$S_{Zrest} = T_{zrest} \times S_{Mean} \quad (8)$$

323  
324  
325  
326

Where  $S_{Mean}$  is the average size of risky and propagation zones and  $T_{zrest}$  is the fourth parameter of the method. Given  $S_{Zrest}$ , the appropriate value of the power of 2 is obtained, such as the size of each remaining zone is as close as possible to  $S_{Zrest}$ . The resulting mesh decomposition on the notched bending beam is illustrated in Figure 18.

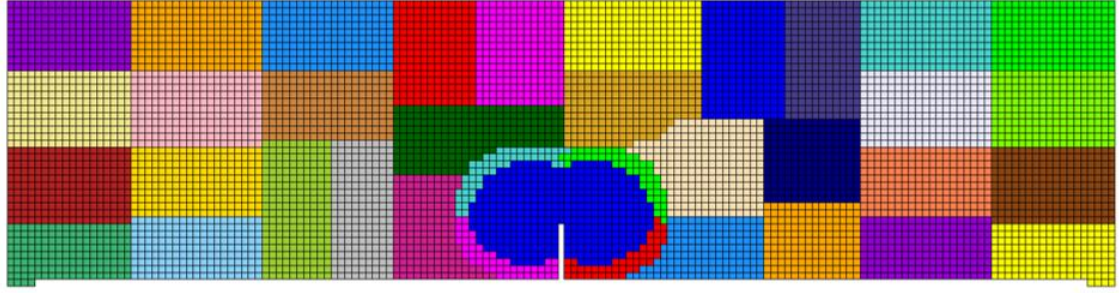


Figure 18 : Final partition of the notched beam for a value of  $T_{zrest} = 1$

327  
328

5. At the end of each of the above four steps, we go through a procedure which consist in eliminating the zones whose dimension ( $S_{zone}$ ) is very small compared to the size of the structure ( $S_{total}$ ). If  $S_{zone} < S_{total} \times T_{minz}$  (with  $T_{minz}$  the fifth parameter of the method), the zone is merged with the neighboring one. This choice is done not to penalize the condensation calculation time, considering too small zones. The value we used for the example above for  $T_{minz}$  is 0.1%.

329  
330  
331  
332  
333  
334

As a conclusion, this partition method, based on the process of damage initiation and propagation, depends on five parameters. The choice of these parameters, which determine the size and the number of the zones, may affect the computation time. In the following, a sensitivity analysis is performed on three test cases to evaluate the influence of each parameter. In this study, the parameter  $p$  which gives the number of loading steps for the verification of the initiation criterion, is also considered, as this parameter is expected to be closely related to the initial mesh decomposition. The sensitivity analysis is thus carried out on the 6 parameters  $\{T_{maxzr}, T_{minz}, T_{zpr}, N_{partpr}, T_{zrest}, p\}$ .

335  
336  
337  
338  
339  
340  
341

### 3.3 SENSITIVITY ANALYSIS

342

This sensitivity analysis is carried out using Uranie [30], which is a software for optimization, meta modeling and uncertainty analysis. The main goal of this study is first to evaluate the individual and crossed effects of the six parameters and then to propose a unique set of "optimal" parameters. The output quantity of interest is the computational time. The sensitivity analysis is performed on 3 test cases, aiming at considering a representative range of applications in terms of geometry and loading. They consist in the 3D prestressed beam (section 2.2) with additional bending, the 2D notched bending beam (section 3.1) and a simplified containment vessel (3D reinforced concrete structure) under internal pressure. 500 simulations are launched on each test case (total of 1500 computations) considering the same variation of parameters. All parameters follow the uniform law over the interval given in Table 3. This interval has been chosen from an initial analysis performed on the notched beam to define "realistic" values.

343  
344  
345  
346  
347  
348  
349  
350  
351  
352

Latin Hypercube Sampling method (LHS) [31] is used to generate the design of experiments. An illustration of the 500 sets of parameters is provided in Figure 19.

353  
354

Table 3 : Interval of variations for the six parameters of the sensitivity analysis (uniform distribution)

Variable	Description [min, max]
$T_{maxzr}$	Max. size of risky zones [2% ; 15%]
$T_{minz}$	Min. size of a zone [0,2% ; 0,5%]
$T_{zpr}$	Size of a propagation zone [1,0 ; 4,0]
$N_{partpr}$	Nb. of parts of a propagation zone [1 ; 8]
$T_{zrest}$	Size of the remaining zones [1,0 ; 4,0]
$p$	Nb. of verification of initiation criterion [1 ; 10]

355  
356

357

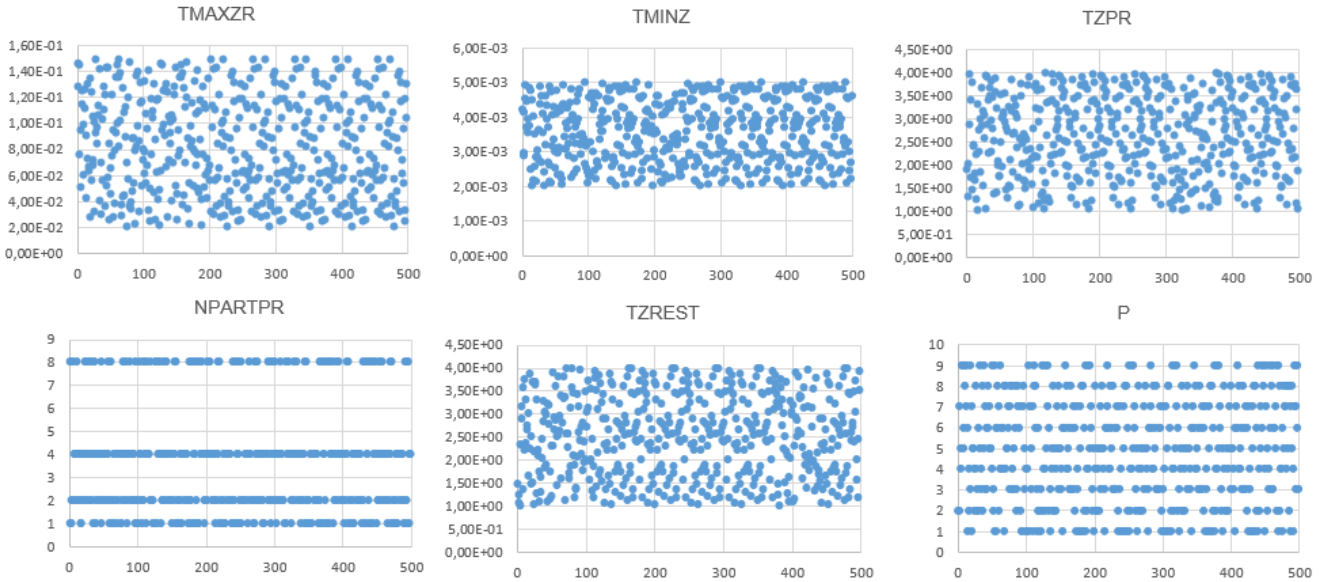


Figure 19 : design-of-experiments of the six input variables

358  
359

360 A sensitivity analysis is then carried out to see the effect of the parameters and to quantify the contribution of each  
 361 parameter on the computation time. Let  $Y = M(X)$  the computation time in function of a random vector  $X$ , defined  
 362 by six input variables  $X = \{T_{maxZR}, T_{minZ}, T_{zpr}, N_{partpr}, T_{zrest}, p\}$ . The aim of this sensitivity analysis is to describe  
 363 how  $Y$  is affected by each input variable or combinations thereof. For this, two sensitivity indices are calculated: the  
 364 first order sensitivity index that represents the effect of the parameter  $X_i$  individually and the total sensitivity index  
 365 that represents the effect of  $X_i$ , taking into account the possible interaction between other parameters.  
 366 The first order sensitivity index is given by [31] :

$$S_i = \frac{Var(E(Y|X_i))}{Var(Y)} \quad (9)$$

367 With  $Var(E(Y|X_i))$  is the expectation of the conditional variance over all possible  $X_i$  values. This index does not  
 368 take into account the possible interaction between the inputs. It can be completed by considering the interaction  
 369 between all the inputs.

370 The total order sensitivity index  $S_{T_i}$  is the sum over all the sensitivity indices involving the input variables:

$$S_{T_i} = \sum_{k \in \#i} S_k = 1 - S_{\bar{i}} \quad (10)$$

371 where  $\#i$  and  $\bar{i}$  represents respectively the group of indices that contains and does not contain the  $i$  index.  
 372 The method chosen to calculate the sensitivity indices is the Sobol's decomposition [32] because it allows  
 373 calculating both the first order and the total sensitivity indexes. Moreover, no hypothesis is needed between the  
 374 inputs and the output (as it is the case in linear regression for example).

### 375 3.3.1 Notched beam in bending

376 The sensitivity analysis is first performed on the 2D notched bending beam. The damage distribution obtained for  
 377 the mesh decomposition provided in Figure 18 is illustrated in Figure 20. It can be compared to the ones in Figure  
 378 12 to validate the method. It is especially noticed that the DI strictly evolves with the damage.

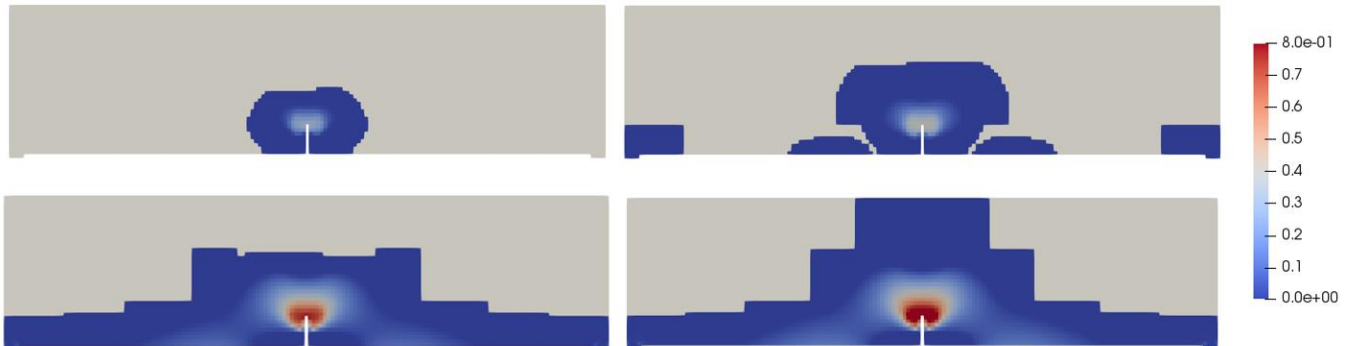
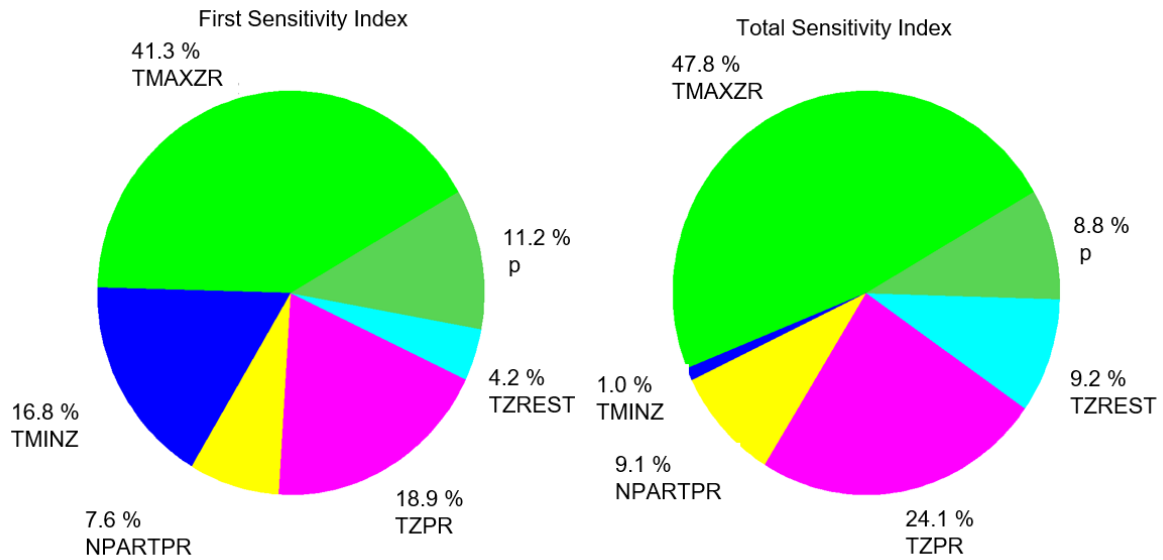


Figure 20 : Evolution of damage inside the DI (grey zones are condensed ones)

379  
380

381

382 The results of the sensitivity analysis are presented in Figure 21. According to the total sensitivity index, the two  
 383 most impacting parameters are the parameters that define the size of a risky zone  $T_{MaxZR}$  (size of risky zones) and  
 384  $T_{Zpr}$  (size of propagation zones). The effect of parameter  $T_{minZ}$  (minimum size of a zone) is negligible. For  
 385 illustration, the computation time ranges from 156 s to 513 s. The computation time associated to the classical finite  
 386 element simulation (without condensation) is 899 s.  
 387

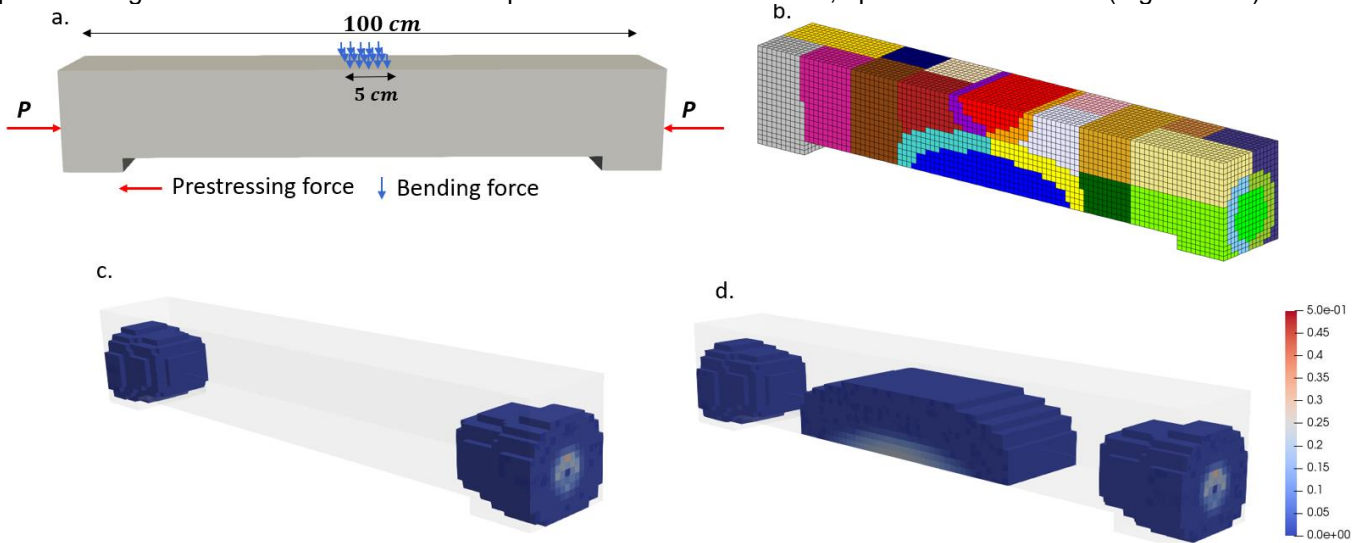


388  
 389 *Figure 21 : Sensitivity indices – notched bending beam*

388  
 389

### 390 3.3.2 Prestressed concrete beam with additional bending

391 The second test case is the 3D prestressed beam presented in part 2.2. A bending loading is added after  
 392 prestressing on a 5 cm width band at the top in the middle of the beam, up to a force of 15 kN (Figure 22-a).



393 *Figure 22 : a – geometry and loads of the prestressed beam in bending ; b – the structure partitioned into 28 zones;*  
 394 *c - damage profile at the end of prestressing; d – damage profile at the end of bending*  
 395

393  
 394  
 395

396 Figure 22 presents an example of automatic mesh decomposition and the resulting damage distributions, after  
 397 prestressing and after the additional bending. It is to be noted that in the mesh partition, risky zones are obtained,  
 398 as expected, at the ends of cables, at the bottom and top in the middle of the beam.

399 Figure 23 presents the results of the sensitivity analysis for this test case. These results show that the two most  
 400 impacting parameters are still  $T_{MaxZr}$  and  $T_{Zpr}$ . Regarding parameter p, the variation between the first order and  
 401 the total sensitivity index clearly indicates a significant interaction between this parameter and the others, which  
 402 confirms previous qualitative observations. The effect of the  $T_{minz}$  parameter whose influence was negligible for  
 403 the bending beam is here more impacting. For illustration, the computation time ranges from 2730 s to 7280 s. The  
 404 computation time associated to the classical finite element simulation (without condensation) is 9210 s.

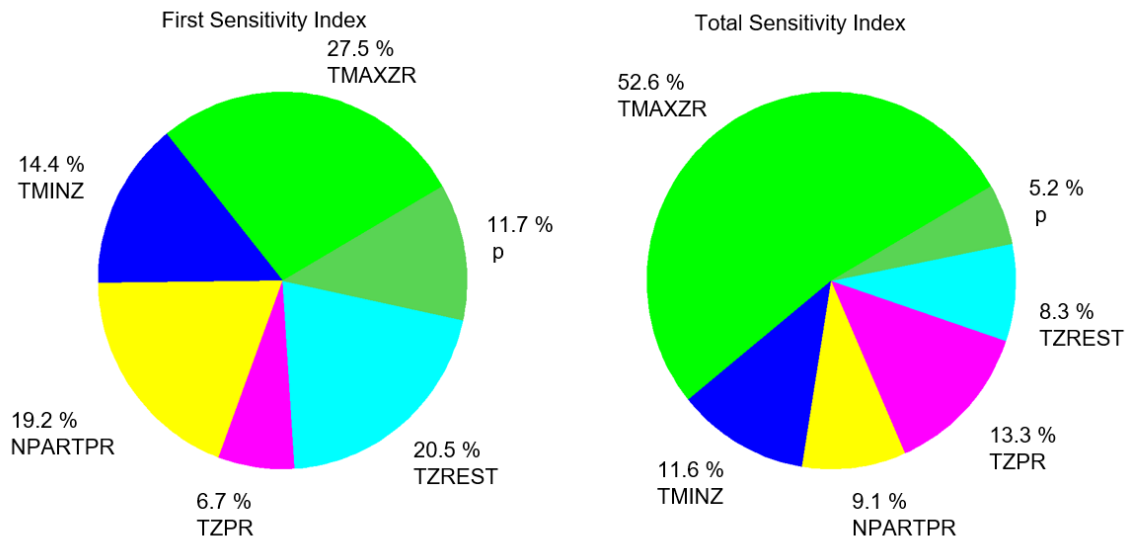


Figure 23 : sensitivity indices – 3D prestressed concrete beam in bending

405  
406

### 407 3.3.3 Simplified containment vessel under pressure (reinforced concrete structure)

408 The last test case is a reinforced concrete cylinder with a hemispherical dome under internal pressure. The structure  
 409 is chosen to be close in its specificities to a nuclear containment vessel [33] and to test the capacity of the ASC  
 410 method to be applied to reinforced concrete applications. It is 13.3 m high, has an external radius of 7.3 m and  
 411 20 cm of thickness. The concrete is meshed with linear cubic finite elements (characteristic size of 20 cm). It  
 412 includes two rectangular openings whose dimensions are respectively 80 × 60 cm and 100 × 60 cm. Reinforcement  
 413 is modeled with 1D bar elements (20 cm length) with an equivalent section  $S = 8.04 \text{ cm}^2$  (3.2 cm of diameter). The  
 414 structure includes 60 hoops and 20 vertical bars in the wall and 20 U-shaped bars passing through the wall and the  
 415 dome (Figure 24 b). “Perfect” kinematic relations ensure the same displacements between steel and concrete.  
 416 Mazars’s damage law is used for concrete with the parameters from [15]. A linear elastic law is chosen for  
 417 reinforcement ( $E = 200 \text{ GPa}$ ;  $\nu = 0,2$ ). The loading is an increasing internal pressure up to  $1 \times 10^5 \text{ Pa}$  and the  
 418 displacements at the bottom of the cylinder are blocked. It is to be noted that a local version of the damage model  
 419 has been done. The non-local regularized one would have required a much finer mesh with an increasing  
 420 computation cost. This point will be addressed in future work through local mesh refinement for example.

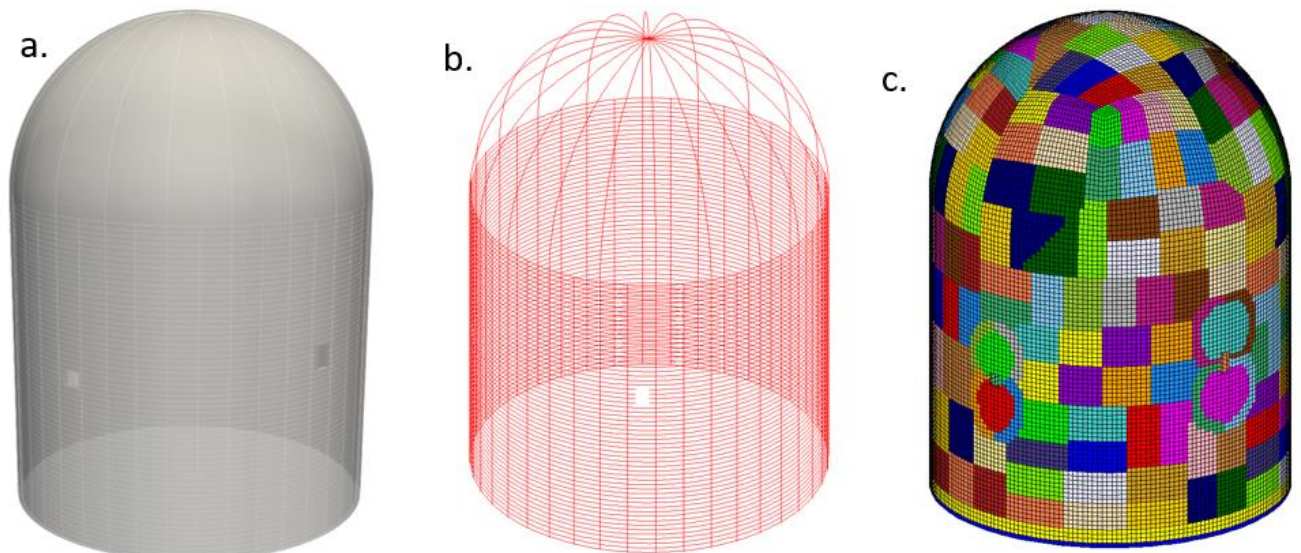
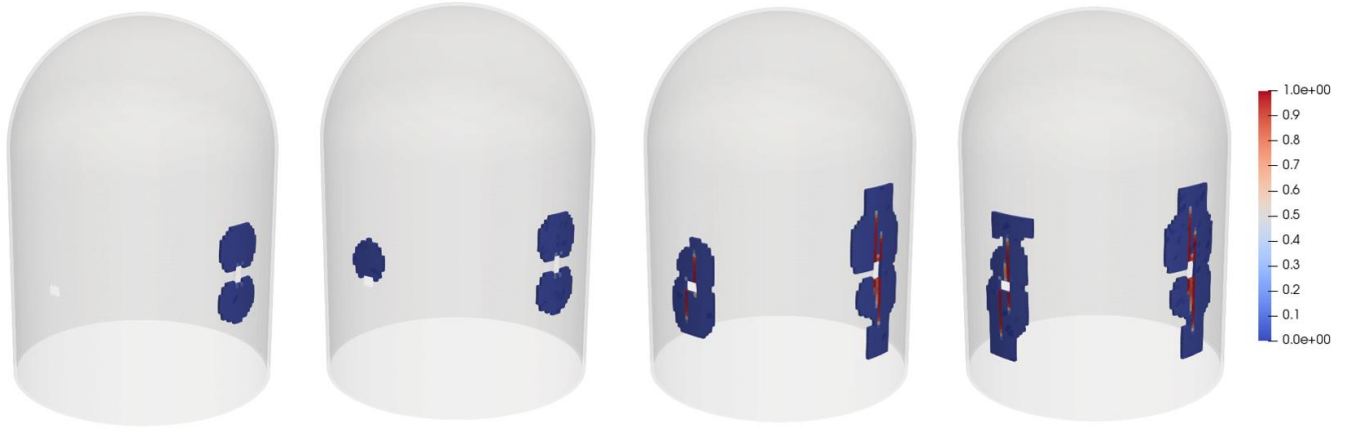


Figure 24 : a – Simplified containment building; b – reinforcement mesh; c – Example of mesh decomposition obtained with the automatic partitioning method

421  
422  
423

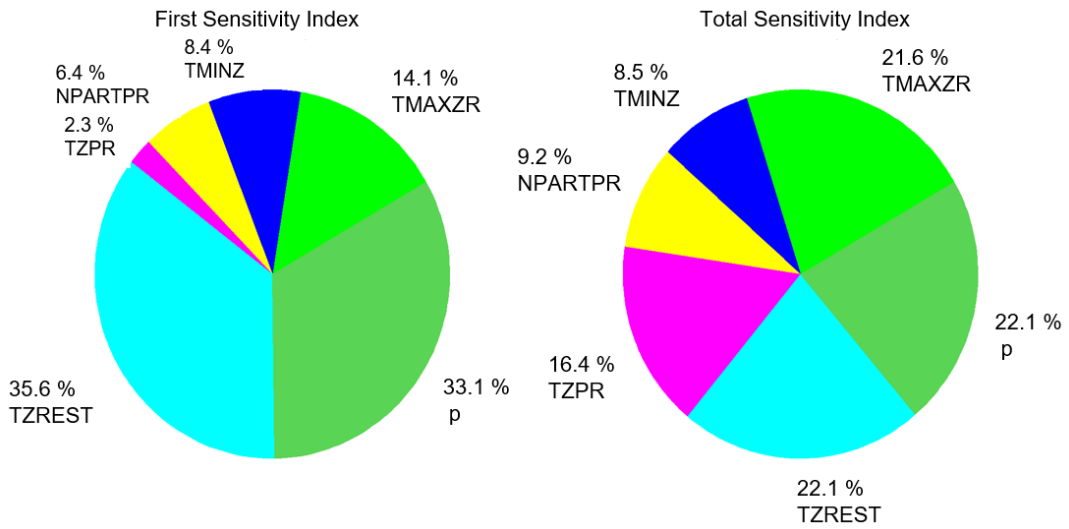
424 Figure 25 presents the damage distributions obtained from the mesh decomposition illustrated in Figure 24c and  
 425 the corresponding evolution of the domain of interest during loading. Two zones first appear at the top and bottom  
 426 of the large opening. Then, damage develops around the small opening. It finally propagates in the vertical  
 427 directions around both openings, which does correspond, as expected, to the weak points of the structure. This  
 428 example illustrates the interest of the proposed mesh decomposition method, as it allows the domain of interest  
 429 to include the maximum possible damage in a smaller number of zones, compared to an arbitrary decomposition into  
 430 equivalent zones.



431  
432

Figure 25 : evolution of damage and of the domain of interest (DI)

433 The results of the sensitivity analysis presented in Figure 26 show that the most impacting parameter here is the  
 434 parameter  $p$  (the number of steps after which the initiation criteria is checked).  $T_{maxZR}$  remains an influencing  
 435 parameter. Parameters  $N_{partpr}$  and  $T_{zrest}$  have also a significant impact.  
 436



437  
438

Figure 26 : sensitivity indices – reinforced concrete cylinder

### 439 3.3.4 Summary of the sensitivity analysis and proposition of an “optimal” set of parameters

440 The results of the sensitivity analysis on three test cases show first that each considered parameter have an impact  
 441 on the calculation time. This impact depends on the test case, the type of loadings and especially on the damage  
 442 propagation. Then, it also indicates that the parameters have significant interaction (especially interaction between  
 443 parameter  $p$  and the initial mesh decomposition).

444 In this section, a unique set is aimed at being proposed in order to optimize the choice of the parameters. To do so,  
 445 the results of the previous 3 x 500 simulations are used. A 500 input vectors is defined:

$$\begin{pmatrix} X_1 \\ \vdots \\ X_i \\ \vdots \\ X_{500} \end{pmatrix} \quad (11)$$

446 Each input vector  $X_i$  is associated to an output per test case  $j$  (computational time:  $t_{i,j}$ ); expressed as:

$$t_{i,j} = M_j(X_i), \text{ with } i : 1 \rightarrow 500 \text{ and } j : 1 \rightarrow 3 \quad (12)$$

447 In order to compare the results on a common scale, each computational time is divided by the computational time  
 448 of the classical finite element simulation (without ASC method) for each test case. The resulting quantity  $R_{i,j}$  thus  
 449 indicates the percentage of a given ASC computation compared to the complete computation time:

$$R_{i,j} = \frac{t_{i,j}}{t_{complete_j}} \quad (13)$$

450 For example, a value  $R_{i,j} = 20\%$  means that the computation using the automatic mesh decomposition with the set  
 451 of parameter  $X_i$ , on the case test  $j$ , is 5 times faster than the complete reference computation (without ASC).  
 452 Finally, to choose the "optimal" set of parameters, for each vector  $X_i$ , the mean value of  $R_{i,j}$  on the 3 test cases is  
 453 computed ( $\bar{R}$ ).

$$\bar{R}_i = \frac{1}{3} \sum_{j:1 \rightarrow 3} R_{i,j} \quad (14)$$

454  
 455 The "optimal" set of parameters set  $X_k$  is the one corresponding to the minimum value of  $\bar{R}$ .

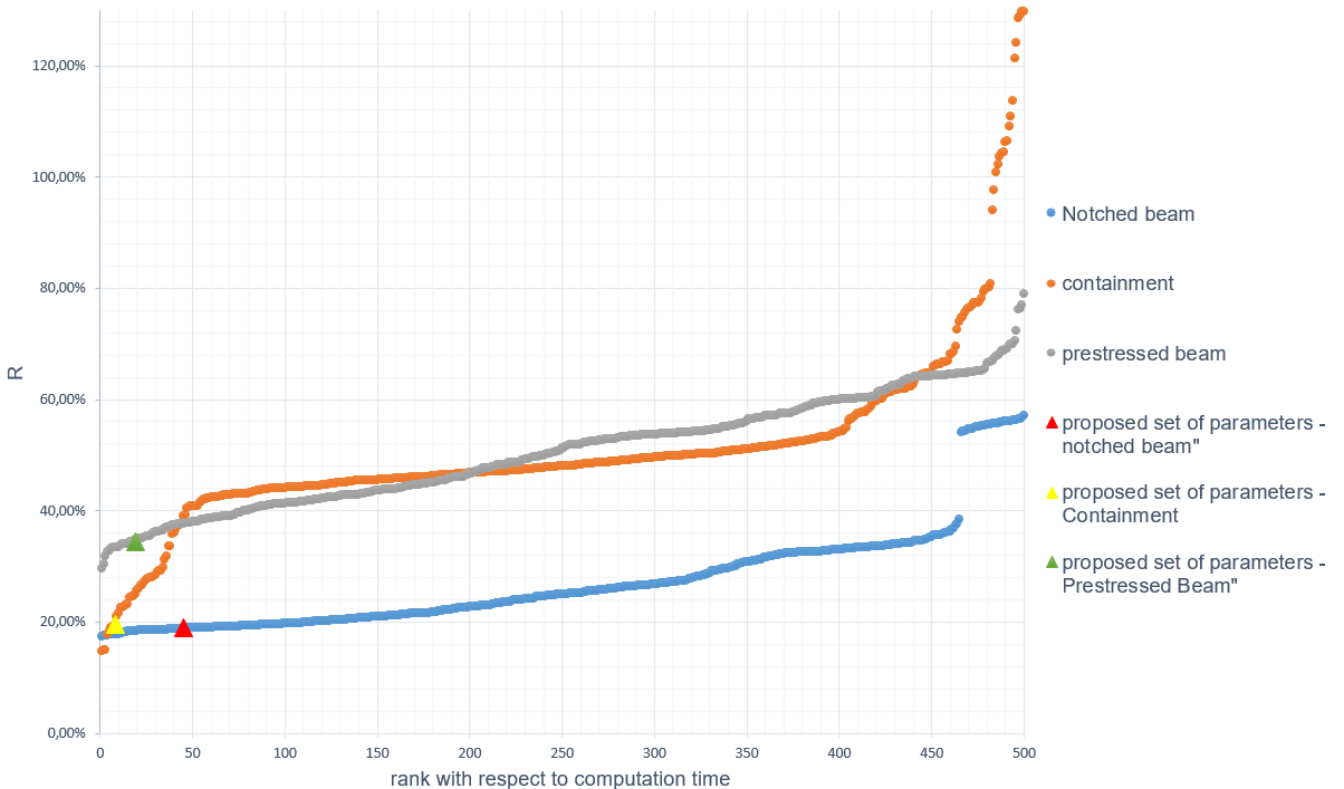
$$\bar{R}_k = \min_{i:1 \rightarrow 500} \bar{R}_i \quad (15)$$

456 The application of this strategy based on the 3x500 simulations gives the following results:

$$X_k = \{2,87 \% ; 0,38\% ; 3,42 ; 2 ; 1,54 ; 6\} \quad (16)$$

$$\bar{R}_k = \frac{19,61 + 18,97 + 34,49}{3} = 24\% \quad (17)$$

457 The result is illustrated in Figure 27 on which the 500 calculations of each test case are sorted in increasing order  
 458 of calculation time (from the fastest to the slowest). It shows that for both beams, the calculation is faster than the  
 459 complete calculation for all considered mesh partition ( $R < 100\%$ ). For the simplified containment, only few mesh  
 460 decomposition lead to a computational time higher than the complete calculation (3%). It particularly demonstrates  
 461 the numerical efficiency of the ASC method on 1500 computations. The results obtained for each test case using  
 462 the proposed "optimal" set of parameters (equation 16) are then positioned on each curve. The results are close to  
 463 the minimum value of the computational time (even if not strictly equal as the goal is to propose a unique set of  
 464 parameters independently of the test case). It should be noted, that even if the three test cases have been chosen  
 465 to be representative a large variety of geometry and loading (at least the ones a containment vessel could face),  
 466 the choice of the "optimal" parameter may have been different if additional test cases had been considered.  
 467 However, it does not question the global strategy that could be enriched if additional loadings were considered.  
 468



469  
 470 *Figure 27 : Evolution of the computational time with the set of parameters for the three tests cases. Sensitivity analysis and*  
 471 *optimal set of parameters*

472 Finally, the proposed automatic mesh decomposition is compared to the results obtained with an initial partitioning  
 473 into equivalent zones on the 2D bending beam (Figure 13). A comparison with the simulation without ASC is also  
 474 included (Figure 28). The automatic partition (the point in dark blue on the Figure 28), based on physical  
 475 interpretation of the damage initiation and propagation and on the sensitivity analysis, is faster than the equivalent  
 476 partitioning, whatever the number of zones. It shows the performance of the newly developed mesh partitioning  
 477 method for the application of the ASC method.

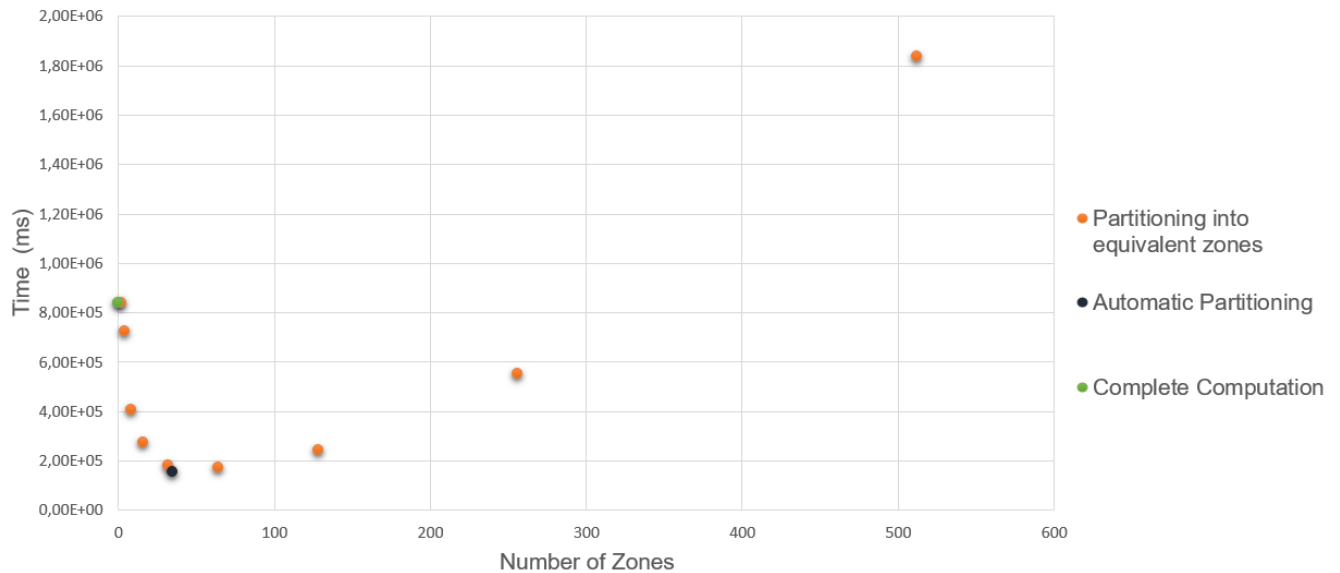


Figure 28 : calculation time as a function of the number of partitioning zones

478  
479

#### 480 4. CONCLUSION AND PERSPECTIVES

481 An ASC method, initially proposed in [15], has been developed to allow reducing the size of large structural  
482 problems to their expected nonlinear part. This method uses the static condensation of Guyan to eliminate the  
483 degrees of freedom of the elastic domain to keep the computational effort on the nonlinear domain of interest only.  
484 As this domain of interest may change (damage propagation or initiation), the condensed domain is checked  
485 regularly and evolves if necessary. It has revealed to be especially efficient in the case of very localized damage  
486 zones.

487  
488 In this contribution, the field of application of the adaptive static condensation (ASC) method has been extended to  
489 take into account the prestressing. In classical finite element methods, this loading requires nonlinear calculations  
490 in several time steps on the total structure, which can be very expensive. After a brief presentation of the needed  
491 developments, the ASC method was successfully applied to the simulation of a prestressed beam. Compared to a  
492 classical simulation, similar results were obtained with a time saving factor of about 15. The efficiency of the method  
493 has thus been demonstrated. It is to be noted that even if this prestressing test is ideal for the efficiency of the  
494 method (damage only localizes in a very limited part of the structure and does not evolve), other computational  
495 performances were obtained on other test cases with “gain factor” up to 5, which remains significant. The  
496 performance is thus obviously dependent on the test cases and on the expected evolution of the damage.

497  
498 As the ASC method supposes an initial mesh decomposition into zones, the effect of this initial decomposition has  
499 been investigated. It has been shown that it can have a significant impact on the computational time. It thus argues  
500 for the development of an automatic mesh decomposition method, rather than the use of manual user partitioning.  
501 The method has been described based on physical interpretation of damage initiation and propagation. It relies on  
502 five geometric parameters whose calibration has been discussed through a sensitivity with 1500 computations. An  
503 optimal set of parameters has been finally proposed, whose results have been discussed. It has proven to be more  
504 efficient than a partitioning into zones of equivalent size, whatever their numbers. It is to be noted that this method  
505 is independent of the mesh size and dimensions of the structure. In addition, it could be used in other applications  
506 where a partitioning of the structure is needed in the order of non-linearity. Finally, it is to be noted that the  
507 optimization process could be enriched in future works with other application cases, either to validate the choice of  
508 the parameters or to optimize their determination.

509  
510 As a perspective, an automatic mesh refinement method could be integrated for the domain of interest in the ASC  
511 method. It will enable to start from a coarse initial mesh to refine only the DI with a mesh density suitable for a non-  
512 local regularized model (mesh size of around one centimeter). The objective would be to reduce the cost of all the  
513 operations related to the condensed domain (condensation and de-condensation) while enabling the application of  
514 a non-local technique whatever the size of the total structure (improvement of the simulation on the simplified  
515 containment building for example).

#### 516 5. ACKNOWLEDGMENTS

517 The authors gratefully acknowledge the partial financial support from EDF R&D for the development and the  
518 analysis of the simulation results.

519  
520

## 6. REFERENCES

- 522 [1] H. Guenter and M. Guenther, Numerical Modeling of Concrete Cracking (Google eBook). Springer, 2011.
- 523 [2] A. K. Noor, "Parallel processing in finite element structural analysis", J. Engineering with Computers, vol. 3,  
524 no. 4, pp. 225–241, 1988.
- 525 [3] C. Bartels, M. Breuer, K. Wechsler, and F. Durst, "Computational fluid dynamics applications on parallel-  
526 vector computers: Computations of stirred vessel flows", J. Computers and fluids, vol. 31, no. 1, pp. 69–97,  
527 2002.
- 528 [4] M. L. Romero, P. F. Miguel, and J. J. Cano, "A parallel procedure for nonlinear analysis of reinforced  
529 concrete three-dimensional frames", J. Computers & Structures, vol. 80, no. 16–17, pp. 1337–1350, 2002.
- 530 [5] N. Abdel-Jabbar, C. Kravaris, B. Carnahan, "Structural analysis and partitioning of dynamic process models  
531 for parallel state estimation", Proceedings of the American Control Conference Philadelphia, Pennsylvania,  
532 1998.
- 533 [6] P. Bassomo, "Contribution à la parallélisation de méthodes numériques à matrices creuses skyline.  
534 Application à un module de calcul de modes et fréquences propres de Systus". Thesis, Université Jean  
535 monnet de Saint-Etienne et de l'école nationale supérieure des mines de Saint-Etienne, 1999.
- 536 [7] M. J. Berger and J. Olinger, "Adaptive mesh refinement for hyperbolic partial differential equations", J.  
537 Computational Physics, vol. 53, no. 3, pp. 484–512, 1984.
- 538 [8] S. Delage Santacreu, "Méthode de raffinement de maillage adaptatif hybride pour le suivi de fronts dans les  
539 écoulements incompressibles", Thesis, L'Université Bordeaux I et l'école doctorale de sciences physiques  
540 et de l'ingénieur, 2006.
- 541 [9] R. J. Guyan, "Reduction of stiffness and mass matrices", AIAA J.3, 1965.
- 542 [10] R. Craig, M. Bampton, "Coupling of Substructures for Dynamic Analyses", AIAA Journal , 1968.
- 543 [11] J. H. Ong, "Automatic masters for eigenvalue economization", J. Earthquake Engineering and Structural  
544 Dynamics, vol. 3, pp. 375-383, 1975.
- 545 [12] A. Y. Leung, "An accurate method of dynamic condensation in structural analysis", International Journal for  
546 Numerical Methods in Engineering, vol. 12, pp. 1705-1715, 1978.
- 547 [13] M. A. Lee, "an approach for efficient , conceptual-level aerospace structural design using the static  
548 condensation reduced basis element method", Thesis, Georgia Institute of Technology , 2018.
- 549 [14] L. S. Moreira, J. B. M. Sousa, and E. Parente, "Nonlinear finite element simulation of unbonded prestressed  
550 concrete beams", Engineering Structures, vol. 170, pp. 167-177, 2017.
- 551 [15] A. Llau, L. Jason, F. Dufour, and J. Baroth, "Adaptive zooming method for the analysis of large structures  
552 with localized nonlinearities", Finite Elements in Analysis and Design, vol. 106, pp. 73-84 ,2015 .
- 553 [16] J. Mazars, F. Hamon, and S. Grange, "A new 3D damage model for concrete under monotonic, cyclic and  
554 dynamic loadings" , Material and Structures , vol. 48, pp. 3779-3793 ,2015.
- 555 [17] Règles BPEL 91 - Règles techniques de conception et de calcul des ouvrages et constructions en béton  
556 précontraint suivant la méthode des états limites. .
- 557 [18] CEA, Description of the finite element code Cast3M, 2021.
- 558 [19] C. Giry, "Modélisation objective de la localisation des déformations et de la fissuration des structures en  
559 béton soumises à des chargements statiques ou dynamiques", Thesis, Université De Grenoble, 2011.
- 560 [20] F. Dufour, G. Legrain, G. Pijaudier-Cabot, A. Huerta, "Estimation of crack opening from a two-dimensional  
561 continuum-based finite element computation", J. International Journal for Numerical and Analytical Methods  
562 in Geomechanics, vol. 36 (16), pp. 1813-1830,2012.
- 563 [21] G. Pijaudier-Cabot and Z. P. Bazant, "Nonlocal damage theory", J. Engineering Mechanics, vol. 113 (10),  
564 pp. 1512-1533,1987.
- 565 [22] F-J. ULM, "Modélisation Elastoplastique avec endommagement du beton de structures", Thesis, Ecole  
566 Nationale des Ponts et Chaussées, 1994.
- 567 [23] M. Ben Oueddou, "Analyse de la diffusion de la précontrainte par la méthode des éléments finis", Colloque  
568 "Matériaux, Sols et Structures" , 2004.
- 569 [24] A. Llau, L. Jason, F. Dufour, and J. Baroth, "Finite element modelling of 1D steel components in reinforced  
570 and prestressed concrete structures", J. Engineering Structures, 2016.
- 571 [25] [R7.01.02], "Modélisation des câbles de précontrainte", Code Aster <http://www.code-aster.org>.
- 572 [26] J. Chen and V. E. Taylor, "ParaPART: Parallel mesh partitioning tool for distributed systems," Lect. Notes  
573 Comput. Sci. (including Subser. Lect. Notes Artif. Intell. Lect. Notes Bioinformatics), vol. 1586, no.  
574 September 1999, pp. 996–1005, 1999, doi: 10.1007/BFb0097984.
- 575 [27] J. Chen and V. E. Taylor, "Mesh Partitioning for Efficient Use of Distributed Systems", IEEE Transactions  
576 On Parallel And Distributed Systems, vol. 12, pp. 111-123, 2000.
- 577 [28] P. Korošec, J. Šilc, and B. Robič, "Solving the mesh-partitioning problem with an ant-colony algorithm", J.  
578 Parallel Computing, vol. 30, pp. 785-801, 2004.
- 579 [29] J. R. Gilbert and R. E. Tarjan, "The analysis of a nested dissection algorithm", J. Numerische Mathematik,  
580 vol. 50, pp. 377-404, 1987.
- 581 [30] CEA, The Uranie platform: an open-source software for optimisation, meta-modelling and uncertainty  
582 analysis.
- 583 [31] Uranie Team, "Methodological reference guide for Uranie v4.4.0", 2020.
- 584 [32] Sobol', "Sensitivity estimates for nonlinear mathematical models", Mathematical and Computer Modelling,

585 1993.  
586 [33] J. Costaz, "Confinement . Enceintes", Techniques de l'ingénieur Conception, construction et exploitation  
587 des réacteurs nucléaires, document data base : TIB204DUO (1997).  
588